Optical Engineering

OpticalEngineering.SPIEDigitalLibrary.org

Soliton building from spontaneous emission by ring-cavity fiber laser using carbon nanotubes for passive mode locking

Younis Mohamed Atiah Al-zahy

SPIE.

Soliton building from spontaneous emission by ring-cavity fiber laser using carbon nanotubes for passive mode locking

Younis Mohamed Atiah Al-zahy*
Misan University, College of Dentistry, Al Amarah 62001, Iraq

Abstract. We investigate the generation of a chirped pulse in a single-mode, ring-cavity, erbium-doped fiber laser employing carbon nanotubes (CNTs) as a saturable absorber (SA). The pulse propagation is simulated using analytical methods to understand and quantify the role of multiple SA properties, particularly in the propagation dynamics of the laser pulse. The soliton solution is obtained on the basis of nonlinear effects, such as gain dispersion, second anomalous group-velocity dispersion, self-phase modulation, and two-photon absorption for a generalized nonlinear Schrodinger equation. The influences of the SA parameter in the range from 0.1 to 0.4 on the chirp, power, and width of the soliton are calculated. A stable, passively mode-locked fiber laser using CNTs as an SA is modeled. In addition, the power, width, chirp, and phase of the soliton pulses can be tuned by choosing suitable SA parameters. [DOI: 10.1117/1.OE.54.1.011005]

Keywords: lasers; soliton; nonlinear optics; fibers laser; passive mode locking; nanotube saturable absorber.

Paper 140866SS received May 28, 2014; revised manuscript received Jul. 8, 2014; accepted for publication Jul. 14, 2014; published online Aug. 8, 2014.

1 Introduction

Single-wall carbon nanotubes (SWCNTs) have attracted much attention in the field of optical communications in recent years because of their ultrafast nonlinear optical properties in the near-infrared region arising from the saturation of excitonic transitions,[1–4] their interesting electronic and optical properties, and several applications in photonics, which include nanometer-scale devices for light generation, photodetection, photovoltaic applications, and application as saturable absorbers (SAs).[5,6] Recent developments in fiber lasers have led to a renewed interest in SAs. CNTs have emerged as a promising technology for the fabrication of SAs.[7] Graphene[8–10]and nanoscale graphite[11,12] materials based on CNTs have attracted much attention because of their high optical nonlinearity and fast recovery time when used as an SA in a mode-locked erbium-doped fiber laser (EDFL) for femtosecond/picosecond pulse generation.[13–18]

Because SWCNTs possess subpicosecond recovery times and broad absorption spectra, active fibers doped with Yb: KLuW operating at a wavelength of 1000 nm,[19] a praseodymium-doped fiber operating at 1300 nm,[20] a ytterbium-doped fiber operating at 1064 nm,[21] and active fibers doped with Er^{+3} operating at 1500 nm have been mode-locked with SWCNT SAs.[22]

Most recent studies on fiber lasers have focused only on the use of CNTs with erbium (Er) fiber lasers for generating short optical pulses at a 22 MHz repetition rate with a 50 kW peak power and a 1.1 ps pulse width[23,24] or a 39 MHz repetition rate with a 3.4 mW peak power and a 115 fs pulse width.[25]

In addition, new SA materials, such as $TI{:}Bi_2Se_3$ and $TI{:}Bi_2Te_3$, have attracted much attention for mode locking of an Er-doped fiber laser and have yielded stable soliton pulses of 1.57 ps at 1564.6 nm and 1.21 ps at 1558 nm, respectively.[26,27] In 2014, Zhang developed an MoS_2-based optical fiber SA device with an operation wavelength suitable for an ytterbium-doped fiber laser and experimentally generated nanosecond dissipative soliton pulses at 1054 nm.[28]

Most previous studies have been experimental, and few theoretical analyses in this field have been presented. Analytical methods may be useful for enabling the study of a wide range of SA parameters. An analytical study involves performing a spatial analysis to obtain new information; a spatial analysis would be difficult to perform experimentally. The theoretical description of pulse shaping and propagation in a fiber ring-cavity laser is based on the generalized nonlinear Schrodinger (NLS) equation. The Schrodinger equation can be solved either analytically or numerically. Analytical methods are more rigorous and provide exact solutions, but they are difficult to use for complex problems. Many articles have been published on the exact solutions to nonlinear wave equations. These include studies of the Backlund transform,[29] the hyperbolic tangent expansion method,[30] the trial function method,[31] the nonlinear transform method,[32] transformed rational function method,[33] and exact 1-soliton solution of the complex modified Korteweg–de Vries equation method.[34]

Numerical methods, such as the split-step Fourier method, have become popular with the development of computing capabilities, although they only give approximate solutions of the NLS equation. [35] Previous studies of the exact solutions to nonlinear wave equations have not dealt with a range of SA parameters for CNTs.

In this paper, we describe and analyze a method for solving the NLS equation that involves the nonlinear effects of CNTs as an SA. The gain in the NLS equation is described

*Address all correspondence to: Younis Mohamed Atiah Al-zahy, E-mail: younisal_zahy72@yahoo.co.uk

by the saturation power of the gain medium, an average small-signal gain, and an average power over the cavity length. The rest of this paper is organized as follows. In Sec. 2, we derive the equations for representing the solitary wave. In Sec. 3.1, we discuss three cases for the chirp parameter and its effect on the generation of a soliton, and we investigate the effect of the SA parameter on the laser power, pulse phase, and pulse width. In Sec. 3.2, we focus on the chaotic behavior of the laser pulse. Section 3.3 considers the stability of the laser pulse; we focus on the phase of the pulse associated with the introduced transformations and present stationary solutions. In Sec. 3.4, we describe the effect of the SA parameter on the dynamic behavior of the chirped pulse.

2 Model Algebraic Equations

In this section, we describe the optical pulse propagation in a fiber laser using the NLS equation for the pulse envelope $\psi(z,T)$ in the presence of mode locking with the use of an SA, including the gain dispersion, losses for the cavity and fiber, gain, group-velocity dispersion (GVD), self-phase modulation (SPM), and two-photon absorption (TPA). This equation can be written as[5]

$$\frac{\partial\psi}{\partial z}+\frac{i}{2}(igT_2^2+\beta_2)\frac{\partial^2\psi}{\partial T^2}=\left[i\gamma+\frac{1}{2}\left(\frac{\delta_{\mathrm{SA}}}{p_{\mathrm{sat}}^{\mathrm{CNT}}}-\frac{g}{p_{\mathrm{sat}}^{\mathrm{Er}}}-\alpha_2\right)\right]|\psi|^2\psi+\frac{1}{2}(g-\alpha-\delta_{\mathrm{SA}})\psi, \tag{1}$$

where $\psi(z,T)$ is the amplitude of the optical pulse, T is the time, z is the propagation distance, α is a coefficient that takes into account material losses in the cavity, δ_{SA} is the SA parameter, α_2 is the TPA parameter, γ is the SPM parameter, β_2 is the second-order dispersion coefficient, $p_{\mathrm{sat}}^{\mathrm{Er}}$ is the saturation power of the gain medium (Er^{+3}), $p_{\mathrm{sat}}^{\mathrm{CNT}}$ is the saturation power of SA (CNTs), and gT_2^2 is a frequency-dependent gain dispersion factor. We assume a chirped pulse given by

$$\psi(z,T)=\chi(z,T)+i\mu(z,T), \tag{2}$$

where

$$\chi(z,T)=\xi\,\mathrm{sech}(\sigma T)\cos\{kz-c\,\log[\cosh(\sigma T)]\}, \tag{3}$$

$$\mu(z,T)=\xi\,\mathrm{sech}(\sigma T)\sin\{kz-c\,\log[\cosh(\sigma T)]\}, \tag{4}$$

where ξ, σ, k, and c are four arbitrary parameters representing the amplitude, width, wave number, and chirp of the pulse, respectively.

When $\partial\psi/\partial z$ is calculated using Eq. (2), it is found to satisfy

$$\frac{\partial\psi(z,T)}{\partial z}=\frac{\partial\chi(z,T)}{\partial z}+i\frac{\partial\mu(z,T)}{\partial z}. \tag{5}$$

The first part of Eq. (5) is given by

$$\frac{\partial\chi(z,T)}{\partial z}=-k\xi\,\mathrm{sech}(\sigma T)\sin\{kz-c\,\log[\cosh(\sigma T)]\}. \tag{6}$$

The second part of Eq. (5) is given by

$$\frac{\partial\mu(z,T)}{\partial z}=k\xi\,\mathrm{sech}(\sigma T)\cos\{kz-c\,\log[\cosh(\sigma T)]\}. \tag{7}$$

We can write an equation for the second derivative of Eq. (2) with respect to T after some algebra, as follows:

$$\frac{\partial\chi(z,T)}{\partial T}=-[\chi(z,T)c+\mu(z,T)]\sigma\,\tanh(\sigma T). \tag{8}$$

Let us assume the new parameters as

$$\Omega=\chi(z,T)c\sigma\,\tanh(\sigma T),\qquad \Gamma=\mu(z,T)\sigma\,\tanh(\sigma T), \tag{9}$$

$$\frac{\partial^2\chi(z,T)}{\partial T^2}=-\left(\frac{\partial\Omega}{\partial T}+\frac{\partial\Gamma}{\partial T}\right). \tag{10}$$

By calculating $\partial\Gamma/\partial T$ and $\partial\Omega/\partial T$, the result is given by

$$\frac{\partial\Gamma}{\partial T}=-\sigma^2c\mu\,\tanh^2(\sigma T)-\sigma^2\chi(z,T)\mathrm{sech}^2(\sigma T)+\sigma^2\chi(z,T)\tanh^2(\sigma T), \tag{11}$$

$$\frac{\partial\Omega}{\partial T}=-\sigma^2c\mu(z,T)\mathrm{sech}^2(\sigma T)+\sigma^2c^2\chi(z,T)\tanh^2(\sigma T)+\sigma^2c\mu(z,T)\tanh^2(\sigma T). \tag{12}$$

Substituting Eqs. (11) and (12) into Eq. (10), we obtain

$$\frac{\partial^2\chi(z,T)}{\partial T^2}=[3c\sigma^2\mu(z,T)\mathrm{sech}^2(\sigma T)+\sigma^2(1-c^2)\chi(z,T)-2c\sigma^2\mu(z,T)+c^2\sigma^2\chi(z,T)\mathrm{sech}^2(\sigma T)-2\sigma^2\chi(z,T)\mathrm{sech}^2(\sigma T). \tag{13}$$

We follow a similar procedure for finding the second derivative of Eq. (13):

$$\frac{\partial^2\mu(z,T)}{\partial T^2}=[-3c\sigma^2\chi(z,T)\mathrm{sech}^2(\sigma T)+\sigma^2(1-c^2)\mu(z,T)+2c\sigma^2\chi(z,T)+c^2\sigma^2\mu(z,T)\mathrm{sech}^2(\sigma T)-2\sigma^2\mu(z,T)\mathrm{sech}^2(\sigma T). \tag{14}$$

Substituting Eqs. (2), (3), (4), (5), (6), (7), (13), and (14) into Eq. (1), after some algebra, we obtain the following equation:

$$ik+\frac{1}{2}(i\beta_2-gT_2^2)[\sigma^2-\sigma^2c^2+c^2\sigma^2\mathrm{sech}^2(\sigma T)-2\sigma^2\mathrm{sech}^2(\sigma T)-3ic\sigma^2\mathrm{sech}^2(\sigma T)+2ic\sigma^2]=i\left(\gamma+i\frac{\alpha_2}{2}\right)|\xi|^2\mathrm{sech}^2(\sigma T)+\frac{1}{2}(g-\alpha-\delta_{\mathrm{SA}})+\frac{1}{2}\left(\frac{\delta_{\mathrm{SA}}}{p_{\mathrm{sat}}^{\mathrm{CNT}}}-\frac{g}{p_{\mathrm{sat}}^{\mathrm{Er}}}\right)|\xi|^2\mathrm{sech}^2(\sigma T). \tag{15}$$

Separating the real and imaginary parts of Eq. (15), we obtain the following two equations:

$$k + \frac{\beta_2}{2}[\sigma^2 - \sigma^2 c^2 + c^2\sigma^2 \,\mathrm{sech}^2(\sigma T) - 2\sigma^2 \,\mathrm{sech}^2(\sigma T)] + \frac{3}{2} g T_2^2 c\sigma^2 \mathrm{sech}^2(\sigma T) - g T_2^2 c\sigma^2 = \gamma|\xi|^2 \,\mathrm{sech}^2(\sigma T), \tag{16}$$

$$g T_2^2[\sigma^2 - \sigma^2 c^2 + c^2\sigma^2 \,\mathrm{sech}^2 - 2\sigma^2 \,\mathrm{sech}^2(\sigma T)] - 3\beta_2 c\sigma^2 \,\mathrm{sech}^2(\sigma T) + 2\beta_2 c\sigma^2 = \alpha_2|\xi|^2 \,\mathrm{sech}^2(\sigma T) - (g - \alpha - \delta_{\mathrm{SA}}) + \left(\frac{\delta_{\mathrm{SA}}}{p_{\mathrm{sat}}^{\mathrm{CNT}}} - \frac{g}{p_{\mathrm{sat}}^{\mathrm{Er}}}\right)|\xi|^2 \,\mathrm{sech}^2(\sigma T). \tag{17}$$

Equating the coefficient of $\mathrm{sech}^2(\sigma T)$ and other parameters in Eq. (16), we obtain the following equations:

$$k + \frac{1}{2}\beta_2(\sigma^2 - \sigma^2 c^2) - g T_2^2 c\sigma^2 = 0, \tag{18}$$

$$\frac{1}{2}\beta_2(\sigma^2 c^2 - 2\sigma^2) + \frac{3}{2} g T_2^2 c\sigma^2 = \gamma|\xi|^2. \tag{19}$$

Equation (17) can be separated into two equations in the form

$$g T_2^2(\sigma^2 - \sigma^2 c^2) + 2\beta_2 c\sigma^2 + (g - \alpha - \delta_{SA}) = 0, \tag{20}$$

$$g T_2^2(\sigma^2 c^2 - 2\sigma^2) - 3\beta_2 c\sigma^2 = \left(\alpha_2 + \frac{\delta_{\mathrm{SA}}}{p_{\mathrm{sat}}^{\mathrm{CNT}}} - \frac{g}{p_{\mathrm{sat}}^{\mathrm{Er}}}\right)|\xi|^2. \tag{21}$$

3 Results and Discussion

The laser configuration consists of a ring cavity. Two types of fibers are used in the cavity: a 6-m piece of Er-doped fiber (EDF) and a standard single-mode fiber (SMF28) with a total net anomalous GVD β_2 of $-0.012\ \mathrm{ps}^2/\mathrm{m}$.

The gain in our fiber laser comes from the EDF, which, when pumped with 980-nm light, exhibits spontaneous emission at 1550 nm. Continuously pumping the gain fiber results in the formation of an initial pulse by amplified spontaneous emission, and the pulse makes several passes through the resonant cavity.[36] It is important to fix the total length of the gain fiber so that the round trip time for a pulse through the resonant cavity basically equals the storage time of the gain fiber and the pulse will return on each successive pass to the gain fiber as the gain fiber has been pumped back up from a depleted state caused by the prior pass. A polarization-independent isolator was spliced into the cavity to force unidirectional operation of the ring. A CNT mode locker was placed between the EDF and the 10% fiber coupler, as shown in Fig. 1.

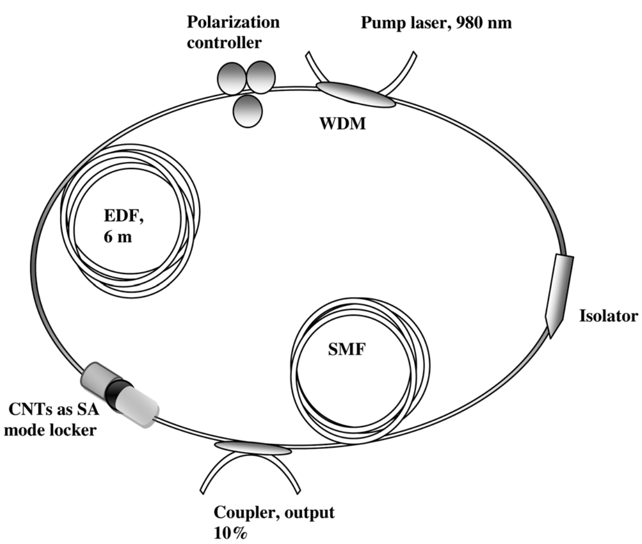

Fig. 1 Schematic of fiber laser components: Er-doped fiber (EDF), single-mode fiber, wavelength-division multiplexer, polarization controller, coupler, and optical isolator.

3.1 *Chirp Dynamics*

To understand the dynamic behavior of the chirp, Eqs. (19) and (21) can be used to find an equation for the chirp.

$$\left[2\gamma g T_2^2 - \left(\alpha_2 + \frac{\delta_{\mathrm{SA}}}{p_{\mathrm{sat}}^{\mathrm{CNT}}} - \frac{g}{p_{\mathrm{sat}}^{\mathrm{Er}}}\right)\beta_2\right]c^2 - 3\left[2\gamma\beta_2 + \frac{1}{2} g T_2^2\left(\alpha_2 + \frac{\delta_{\mathrm{SA}}}{p_{\mathrm{sat}}^{\mathrm{CNT}}} - \frac{g}{p_{\mathrm{sat}}^{\mathrm{Er}}}\right)\right]c - 2\left[2\gamma g T_2^2 - \left(\alpha_2 + \frac{\delta_{\mathrm{SA}}}{p_{\mathrm{sat}}^{\mathrm{CNT}}} - \frac{g}{p_{\mathrm{sat}}^{\mathrm{Er}}}\right)\beta_2\right] = 0. \tag{22}$$

After some algebra, we obtain the following equation:

$$c^2 - 3\frac{\left[2\gamma\beta_2 + \frac{1}{2} g T_2^2\left(\alpha_2 + \frac{\delta_{\mathrm{SA}}}{p_{\mathrm{sat}}^{\mathrm{CNT}}} - \frac{g}{p_{\mathrm{sat}}^{\mathrm{Er}}}\right)\right]}{\left[2\gamma g T_2^2 - \left(\alpha_2 + \frac{\delta_{\mathrm{SA}}}{p_{\mathrm{sat}}^{\mathrm{CNT}}} - \frac{g}{p_{\mathrm{sat}}^{\mathrm{Er}}}\right)\beta_2\right]} c - 2 = 0. \tag{23}$$

We can rewrite the above equation as

$$c^2 - mc - n = 0, \tag{24}$$

where the parameters m and n are given by

$$m = -3\left[\frac{2\gamma\beta_2 + \frac{1}{2} g T_2^2\left(\alpha_2 + \frac{\delta_{\mathrm{SA}}}{p_{\mathrm{sat}}^{\mathrm{CNT}}} - \frac{g}{p_{\mathrm{sat}}^{\mathrm{Er}}}\right)}{2\gamma g T_2^2 - \left(\alpha_2 + \frac{\delta_{\mathrm{SA}}}{p_{\mathrm{sat}}^{\mathrm{CNT}}} - \frac{g}{p_{\mathrm{sat}}^{\mathrm{Er}}}\right)\beta_2}\right], \qquad n = -2. \tag{25}$$

It is easy to show that the chirp parameter is

$$c = \frac{m}{2} \pm \sqrt{\frac{m^2 - 4n}{4}}, \tag{26}$$

$$c = \frac{3}{2}\frac{\left[2\gamma\beta_2 + \frac{1}{2} g T_2^2\left(\alpha_2 + \frac{\delta_{\mathrm{SA}}}{p_{\mathrm{sat}}^{\mathrm{CNT}}} - \frac{g}{p_{\mathrm{sat}}^{\mathrm{Er}}}\right)\right]}{\left[2\gamma g T_2^2 - \left(\alpha_2 + \frac{\delta_{\mathrm{SA}}}{p_{\mathrm{sat}}^{\mathrm{CNT}}} - \frac{g}{p_{\mathrm{sat}}^{\mathrm{Er}}}\right)\beta_2\right]} \pm \sqrt{\frac{9}{4}\left[\frac{2\gamma\beta_2 + \frac{1}{2} g T_2^2\left(\alpha_2 + \frac{\delta_{\mathrm{SA}}}{p_{\mathrm{sat}}^{\mathrm{CNT}}} - \frac{g}{p_{\mathrm{sat}}^{\mathrm{Er}}}\right)}{2\gamma g T_2^2 - \left(\alpha_2 + \frac{\delta_{\mathrm{SA}}}{p_{\mathrm{sat}}^{\mathrm{CNT}}} - \frac{g}{p_{\mathrm{sat}}^{\mathrm{Er}}}\right)\beta_2}\right]^2 + 2}. \tag{27}$$

We can use Eq. (27) to investigate the chirp parameter; we discuss the three cases separately.

Case 1: The solution of Eq. (27) is called the symmetric state and exists only for $m^2-4n>0$. The chirp parameter is real and indicates that the pulse-formed soliton will propagate without changes in its shape; the pulse is stable.

Case 2: When $m^2-4n=0$, the chirp is given by $c=m/2$, indicating that the frequency is always shifted (chirping always occurs) unless the pulse forms a soliton.

Case 3: The solution of Eq. (27) represents an antisymmetric state and exists for all $m^2-4n<0$. In this case, the chirp parameter is purely imaginary, and it is impossible to obtain the soliton from a pulse because the antisymmetric states are unstable.

From the condition that the chirp parameter is real, we obtain

$$\frac{9}{4}\left[\frac{2\gamma\beta_2+\frac{1}{2}gT_2^2\left(\alpha_2+\frac{\delta_{\mathrm{SA}}}{p_{\mathrm{sat}}^{\mathrm{CNT}}}-\frac{g}{p_{\mathrm{sat}}^{\mathrm{Er}}}\right)}{2\gamma gT_2^2-\left(\alpha_2+\frac{\delta_{\mathrm{SA}}}{p_{\mathrm{sat}}^{\mathrm{CNT}}}-\frac{g}{p_{\mathrm{sat}}^{\mathrm{Er}}}\right)\beta_2}\right]^2+2\geq 0. \tag{28}$$

For a fiber laser employing CNTs, gT_2^2, β_2, α_2, $g/p_{\mathrm{sat}}^{\mathrm{Er}}$, and γ play important roles in the evolution of passive mode-locked pulses and should be included.

According to Eq. (28), we obtain

$$\delta_{\mathrm{SA}}\geq\frac{2\left(\beta_2+i\frac{4}{3}\sqrt{2}gT_2^2\right)}{\left(\frac{1}{2}gT_2^2+i\frac{2}{3}\sqrt{2}\beta_2\right)}\gamma p_{\mathrm{sat}}^{\mathrm{CNT}}-\left(\alpha_2-\frac{g}{p_{\mathrm{sat}}^{\mathrm{Er}}}\right)p_{\mathrm{sat}}^{\mathrm{CNT}}. \tag{29}$$

When a complex number $(\beta_2+i(4/3)\sqrt{2}gT_2^2)$ is multiplied by its conjugate, the result is

$$\delta_{\mathrm{SA}}\geq\frac{\frac{41}{9}gT_2^2\beta_2}{\left(\frac{1}{4}g^2T_2^4+\frac{8}{9}\beta_2^2\right)}\gamma p_{\mathrm{sat}}^{\mathrm{CNT}}-i\frac{\frac{4}{3}\sqrt{2}(\beta_2^2-g^2T_2^4)}{\left(\frac{1}{4}g^2T_2^4+\frac{8}{9}\beta_2^2\right)}\gamma p_{\mathrm{sat}}^{\mathrm{CNT}}-\left(\alpha_2-\frac{g}{p_{\mathrm{sat}}^{\mathrm{Er}}}\right)p_{\mathrm{sat}}^{\mathrm{CNT}}. \tag{30}$$

The SA parameter δ_{SA} must be real; therefore, $4/3\sqrt{2}(\beta_2^2-g^2T_2^4)=0$, and

$$\delta_{\mathrm{SA}}\geq\left(4\gamma+\frac{g}{p_{\mathrm{sat}}^{\mathrm{Er}}}-\alpha_2\right)p_{\mathrm{sat}}^{\mathrm{CNT}}. \tag{31}$$

This equation shows that the condition that the saturable absorption parameter δ_{SA} must yield a real chirp parameter c can be related to the stable soliton.

According to Eq. (21) and the condition $|\xi|^2\geq 0$, we obtain

$$\alpha_2+\frac{\delta_{\mathrm{SA}}}{p_{\mathrm{sat}}^{\mathrm{CNT}}}-\frac{g}{p_{\mathrm{sat}}^{\mathrm{Er}}}\leq\frac{1}{T_{\mathrm{FWHM}}^2}(gT_2^2c^2-3\beta_2c-2). \tag{32}$$

This clearly illustrates that the nonlinear behavior is altered from saturable absorption to TPA as the intensity of the optical pulse increases. The transformation from saturable absorption to TPA suggests that another nonlinear process occurs and becomes dominant. This interesting effect can be used for optical pulse compression; the above behavior of the optical pulse depends on the values of the parameters gT_2^2, β_2, α_2, $\delta_{\mathrm{SA}}/p_{\mathrm{sat}}^{\mathrm{CNT}}$, $g/p_{\mathrm{sat}}^{\mathrm{Er}}$, and γ.

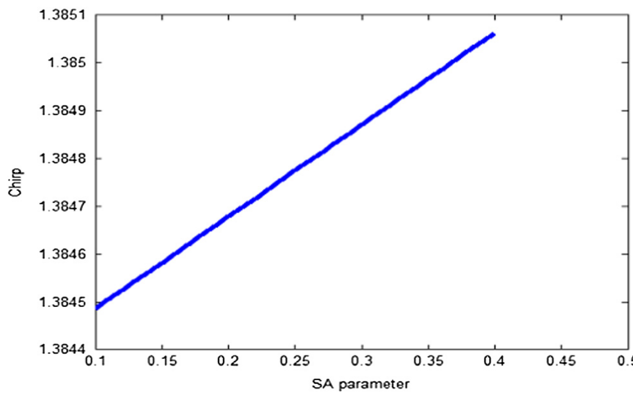

Fig. 2 Chirp versus saturable absorption parameter δ_{SA}.

We can use Eq. (27) to calculate the pulse chirp for δ_{SA} values between 0.1 and 0.4. Figure 2 shows the changes in the chirp as a function of δ_{SA}; the chirp increases linearly with δ_{SA}.

3.2 *Unstable Laser Pulse*

Analytical simulations of pulses that grow through a 5-m fiber ring without a saturable absorption mode locker show that each input pulse develops an internal substructure consisting of many subpulses with widths on the order of femtoseconds. Figure 3 shows the evolution toward a parabolic shape when a "sech" pulse is amplified over the 5-m length of the fiber laser; the position and width of the subpulses change continuously in an apparently random manner. Changing the anomalous GVD values by varying the length of the SMF, therefore, will cause the total cavity dispersion to vary as well.[37] Figure 3 shows that each pulse still develops an internal substructure that depends on the frequencies of the photon laser through the ring resonator, and the pulse power also varies from pulse to pulse and exhibits chaotic behavior as the phase is varied in the cavity resonance.

3.3 *Stable Pulse (Soliton)*

The solution of Eq. (2) provides a shortcut to understanding the behavior of pulse laser propagation through an Er^{+3} ring cavity 6 m in length with a saturable absorption mode locker. In this section, we concentrate on the effects of the absorption parameter on the characteristics of the laser pulse; the absorption parameter is tuned in a wide range from 0.1 to 0.4 (Ref. 38) by varying the thickness of the CNTs. First, by joining Eqs. (20) and (27), we find the soliton width σ. Second, from Eq. (18), we obtain the wave number of the soliton, k. Third, from Eq. (21), we can obtain the soliton power. Fourth, we substitute the soliton width, soliton power, and wave number into Eqs. (3) and (4) and algebraically combine the resulting equations with Eq. (2) to obtain a solitary wave equation describing the dynamics and propagation of optical pulses in a 6-m-long EDFL.

Figure 4 shows the three-dimensional soliton pulse propagation in an EDFL, and Fig. 5 shows the sech pulse profile when the system parameters are $\gamma=0.012\ (\mathrm{Wm})^{-1}$, $\beta_2=-0.012\ \mathrm{ps}^2/\mathrm{m}$, $\alpha_2=0.3$, $T_2=0.047$ ps, $\delta_{\mathrm{SA}}=0.1$,

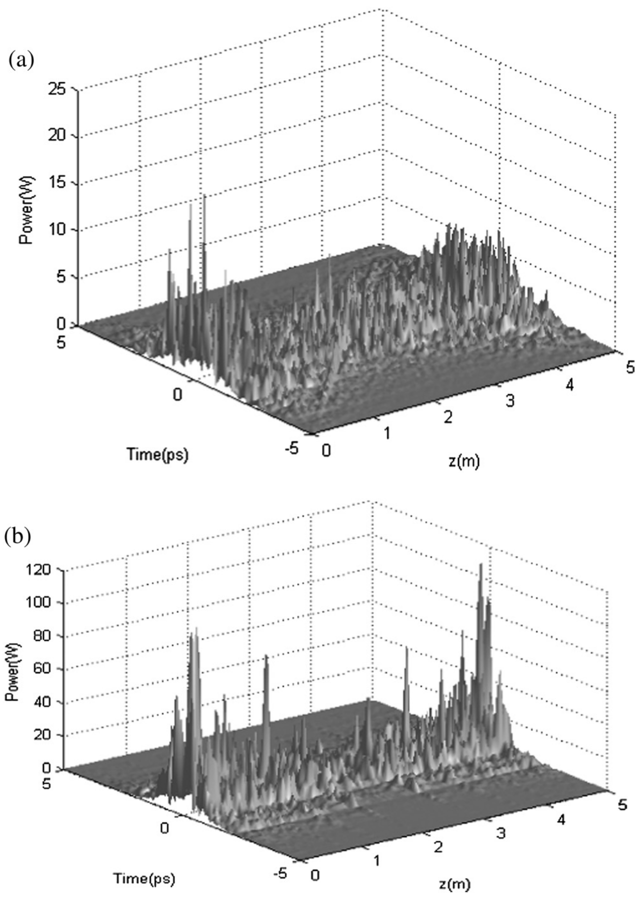

Fig. 3 Evolution of substructure in a 5 m ring resonator when pulses grow from spontaneous emission with group-velocity dispersion: (a) $\beta_2 = -0.014\ \mathrm{ps}^2/\mathrm{m}$, (b) $\beta_2 = -0.012\ \mathrm{ps}^2/\mathrm{m}$. Other parameters are $\gamma = 0.012\ (\mathrm{Wm})^{-1}$, $\alpha_2 = 0.3$, $T_2 = 0.047$ ps, $\alpha = 0.17823\ \mathrm{m}^{-1}$, and $g = 0.78275\ \mathrm{m}^{-1}$.

$\alpha = 0.178\ \mathrm{m}^{-1}$, $p_{\mathrm{sat}} = 210$ W, and $g = 0.782\ \mathrm{m}^{-1}$.[38] The power of the soliton grows exponentially once the power of the pulse exceeds a threshold value, where, at $z = 10$ cm, the power of the soliton is 0.007 W, and a picosecond optical pulse is amplified in the EDFL until the gain saturates at $z = 4$ m with a power of 1.2 W.

Figures 6(a) and 6(b) show the variation in the soliton phase with time and with the length of the fiber laser, respectively, according to the phase equation $\varphi = kz - c\ \log[\cosh(\sigma T)]$, for a fixed length of $z = 4$ m. The phase changes with time as a cosine wave with a range of 1 to -1, as shown in Fig. 6(a). The wave number k; in the phase equation depends on β_2, gT_2^2, c, and T_{FWHM}, as shown in the following equation:

$$k = \frac{1}{2T_{\mathrm{FWHM}}^2}(\beta_2 c^2 + 2\ gT_2^2 c - \beta_2), \tag{33}$$

where

$$T_{\mathrm{FWHM}} = \frac{1.76}{\sigma}. \tag{34}$$

Let us consider the case in which the soliton phase varies linearly along the fiber length, as shown in Fig. 6(b). At $z = 0$ m, the soliton phase is $\varphi = -0.7$, and the phase reaches a maximum value of $\varphi = -0.57$ when $z = 6$ m. Clearly, the values of the phase play an important role in building the soliton from spontaneous emission of the Er^{+3} fiber laser.

3.4 *Effect of SA on Soliton Behavior*

First, we explain the control of the pulse width in a mode-locked fiber laser in which CNTs act as an SA by adjusting the laser's intracavity SA parameter. Equation (35) shows that the SA parameter can vary with T_{FWHM}.

$$\delta_{\mathrm{SA}} = \frac{1}{T_{\mathrm{FWHM}}^2}(2\beta_2 c + gT_2^2 - gT_2^2 c^2) + (g - \alpha). \tag{35}$$

Figure 7(a) shows the soliton width (FWHM) as a function of δ_{SA}. The soliton width increases with δ_{SA}.

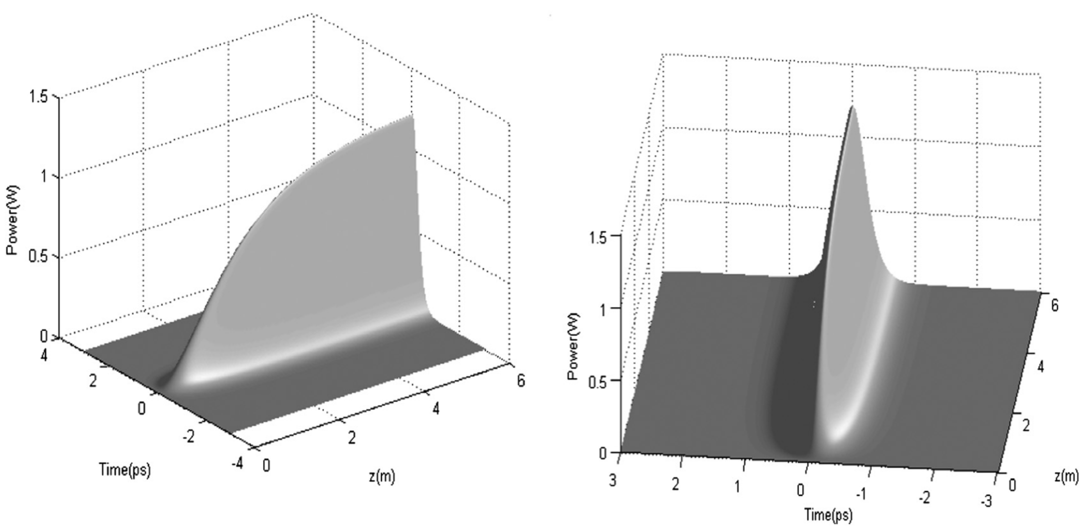

Fig. 4 Soliton growth from spontaneous emission with erbium-doped fiber laser parameters of $\gamma = 0.012\ (\mathrm{Wm})^{-1}$, $\beta_2 = -0.012\ \mathrm{ps}^2/\mathrm{m}$, $\alpha_2 = 0.3$, $T_2 = 0.047$ ps, $\alpha = 0.17823\ \mathrm{m}^{-1}$, $g = 0.78275\ \mathrm{m}^{-1}$, $\delta_{\mathrm{SA}} = 0.1$ and $p_{\mathrm{sat}} = 210$ W.

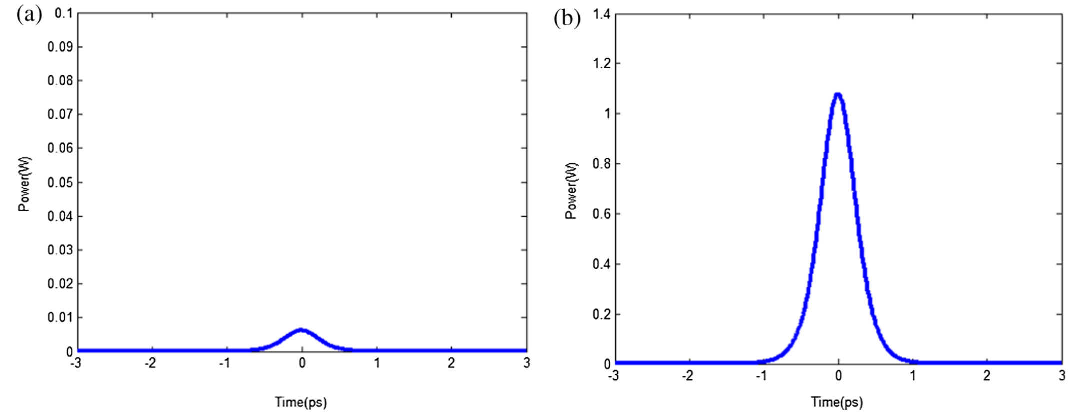

Fig. 5 Profiles of parabolic pulse at (a) $z = 0.1$ m and (b) $z = 6$ m.

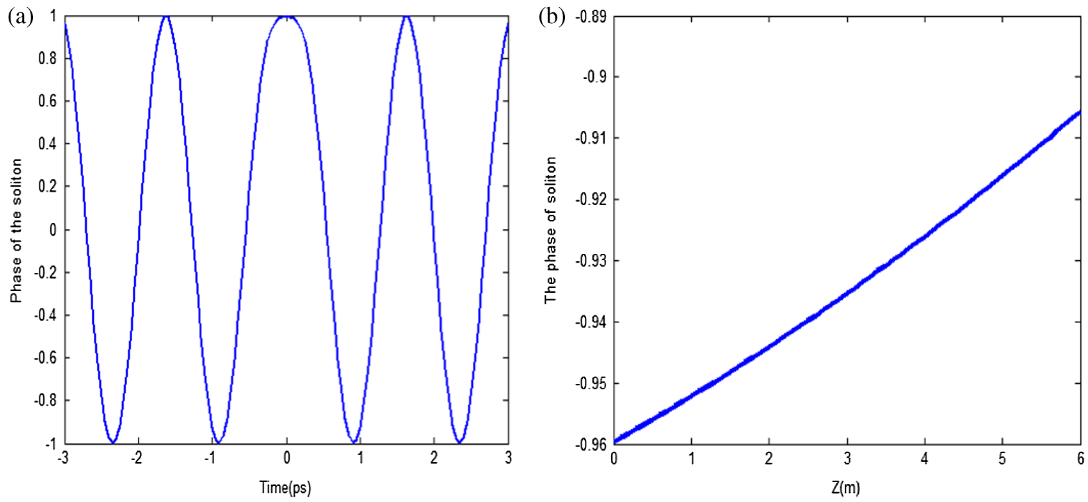

Fig. 6 Soliton phase plotted as a function of (a) time and (b) fiber length.

Second, we focus on the soliton power and SA parameter. Increasing δ_{SA} reduces the soliton power, as can be inferred from Eq. (36). Furthermore, it is easy to show that δ_{SA} depends on p_{sat} and p and refers to the evolution of the building pulse toward a soliton as its width decreases and peak power increases, as shown in Fig. 7(b).

$$\delta_{SA} = \frac{p_{sat}^{CNT}}{p} \frac{T_2^2}{T_{FWHM}^2} g(c^2 - 2) - 3 \frac{p_{sat}^{CNT}}{p} \frac{\beta_2}{T_{FWHM}^2} c + (g - \alpha_2 p_{sat}^{CNT}). \tag{36}$$

Figures 8(a) and 8(b) show the effect of changing the δ_{SA} on the shape of the soliton; the soliton is repeatedly

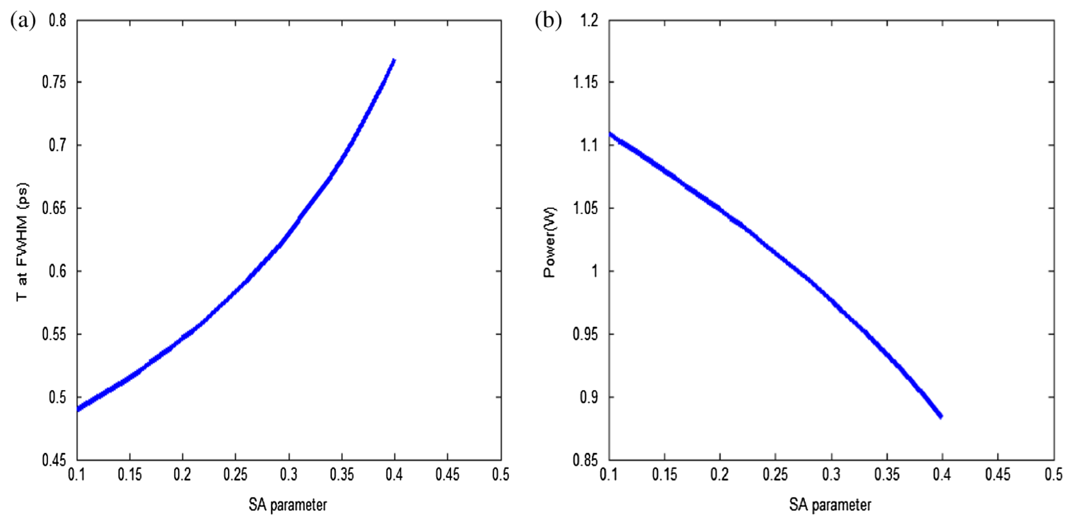

Fig. 7 (a) width of soliton and (b) output power versus δ_{SA}.

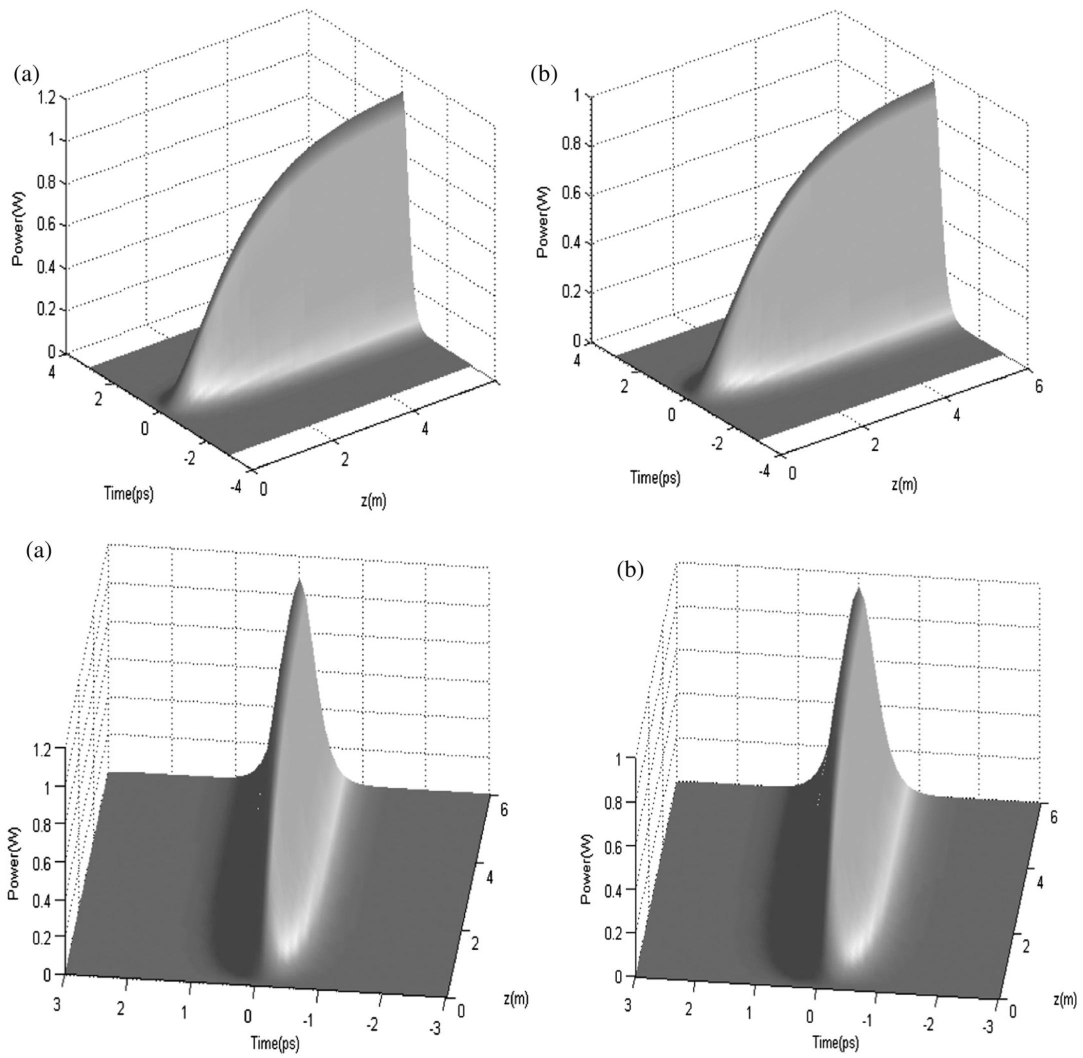

Fig. 8 Soliton growth from spontaneous emission: (a) $\delta_{\mathrm{SA}} = 0.2$, (b) $\delta_{\mathrm{SA}} = 0.3$.

propagated around the laser cavity until a steady state is reached. The soliton power grows exponentially along the fiber length. SAs can also be used to filter sidebands associated with solitons because sidebands can be selectively transferred to the lossy core because of their low power level.

The soliton power in the fiber resonators is evident from Eq. (37). Note that the power depends on the GVD β_2, gain dispersion gT_2^2, chirp c, SPM parameter γ, and soliton width T_{FWHM}.

$$|\xi|^2 = \frac{1}{2\gamma T_{\mathrm{FWHM}}^2}(-\beta_2 c^2 + 3\ gT_2^2 c + \beta_2), \tag{37}$$

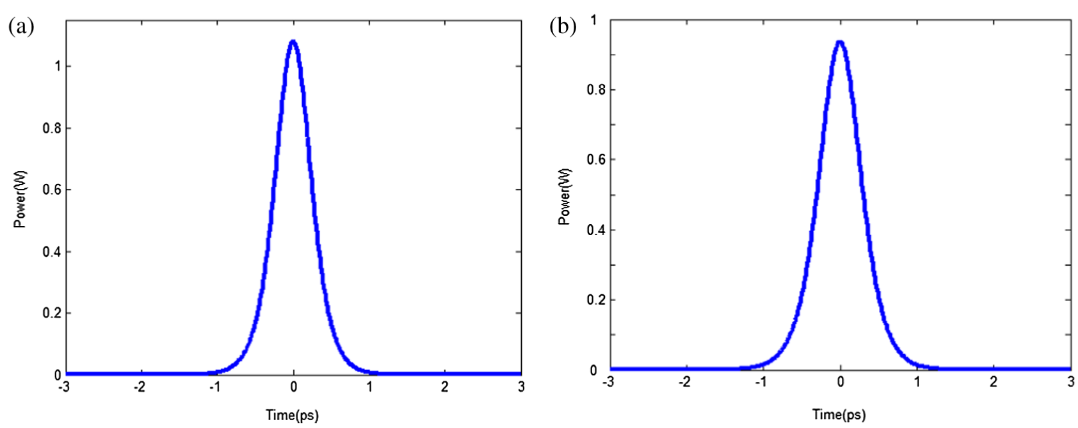

Fig. 9 Profile of optical pulse that forms a soliton for (a) $\delta_{\mathrm{SA}} = 0.2$ and (b) $\delta_{\mathrm{SA}} = 0.3$.

$$T_{\mathrm{FWHM}} = 1.76\sqrt{\frac{-gT_2^2(1-c^2) - 2\beta_2 c}{(g - \alpha - \delta_{\mathrm{SA}})}}. \tag{38}$$

It is evident from Eqs. (37) and (38) that the parameters ξ and T_{FWHM} can have real, positive values or imaginary values, depending on the value under the radical of Eq. (38). ξ and T_{FWHM} play an important role in stable optical pulses; if ξ and T_{FWHM} are real, the optical pulse forms a soliton. Figures 9(a) and 9(b) show that the output pulse forms a soliton and becomes broader with increasing δ_{SA} and decreasing power.

4 Conclusions

We highlighted four important properties: the power, width, chirp, and phase of the pulse laser on the basis of a mathematical model for fiber lasers with ring cavities and CNTs as an SA mode locker. For values of $\gamma = 0.012\ (\mathrm{Wm})^{-1}$, $\beta_2 = -0.012\,\mathrm{ps}^2/\mathrm{m}$, $\alpha_2 = 0.3$, $T_2 = 0.047\,\mathrm{ps}$, $\alpha = 0.17823\,\mathrm{m}^{-1}$, $g = 0.78275\ \mathrm{m}^{-1}$, and $p_{\mathrm{sat}} = 210$ W, ξ and T_{FWHM} must be positive and real to guarantee stable pulse propagation (a soliton). In this paper, we argued that $\delta_{\mathrm{SA}} = 0.1$ is the best value for generating solitons at a power of $\sim$1.2 W and width of $\sim$0.5 ps. The second major finding was that the soliton power decreases as the SA parameter δ_{SA} increases, but that the soliton width increases with increasing δ_{SA}. Furthermore, different δ_{SA} values yield different soliton characteristics; this provides a convenient method for tuning the properties of the generated soliton in ring-cavity fiber lasers, where the properties of the SA parameter depend on the size of the CNTs; therefore, the TPA from a thinner diameter of the CNTs could destroy the stability of mode-locked pulse formation. Consequently, a thicker diameter of the CNTs with less nonlinearity was identified as the mode locker to reduce the TPA, where both gain dispersion and two-photon absorption provide such a loss mechanism, and hence, the TPA plays an important role in establishing the soliton. These observations are in agreement with numerical simulations.[38] Moreover, our results for the parabolic shape of the pulse and the behavior of the laser pulse propagation through the fiber laser exhibit good agreement with previous studies.[39–43]

Acknowledgments

The author is grateful for the assistance of Professor Dr. Kavintheran Thambiratnam and Professor Dr. Zoltan Varallyay.

References

1. S. Y. Set et al., "Laser mode locking using a saturable absorber incorporating carbon nanotubes," *J. Lightwave Technol.* **22**(1), 51–56 (2004).
2. F. Bonaccorso et al., "Graphene photonics and optoelectronics," *Nat. Photonics* **4**(9), 611–622 (2010).
3. G. Sobon, J. Sotor, and K. M. Abramski, "Passive harmonic mode-locking in Er-doped fiber laser based on graphene saturable absorber with repetition rates scalable to 2.22 GHz," *Appl. Phys. Lett.* **100**(16), 161109–161112 (2012).
4. Q. Bao and K. P. Loh, "Graphene photonics, plasmonics, and broad-band opto-electronic devices," *ACS Nano* **6**(5), 3677–3694 (2012).
5. G. R. Lin and Y. C. Lin, "Directly exfoliated and imprinted graphite nano-particle saturable absorber for passive mode-locking erbium-doped fiber laser," *Laser Phys. Lett.* **8**(12), 880–886 (2011).
6. Y. H. Lin and G. R. Lin, "Free-standing nano-scale graphite saturable absorber for passively mode-locked erbium doped fiber ring laser," *Laser Phys. Lett.* **9**(5), 398–404 (2012).
7. K. S. Novoselov et al., "Electric field effect in atomically thin carbon films," *Science* **306**(5696), 666–669 (2004).
8. K. S. Novoselov et al., "Two-dimensional gas of massless Dirac fermions in graphene," *Nature* **438**(7065), 197–200 (2005).
9. Y. C. Chen et al., "Ultrafast optical switching properties of single-wall carbon nanotube polymer composites at 1.55 μm," *Appl. Phys. Lett.* **81**(6), 975–977 (2002).
10. T. Hertel et al., "Charge-carrier dynamics in single-wall carbon nanotube bundles: a time-domain study," *Appl. Phys. A* **75**(4), 449–465 (2002).
11. S. Tatsuura et al., "Semiconductor carbon nanotubes as ultrafast switching materials for optical communication," *Adv. Mater.* **15**(6), 534–537 (2003).
12. J.-S. Lauret et al., "Ultrafast carrier dynamics in single-wall carbon nanotubes," *Phy. Rev. Lett.* **90**(5), 057404 (2003).
13. H. Kataura et al., "Optical properties of single-wall carbon nanotubes," *Synth. Met.* **103**(1–3), 2555–2558 (1999).
14. P. Avouris, M. Freitag, and V. Perebeinos, "Carbon-nanotube photonics and optoelectronics," *Nat. Photonics* **2**(6), 341–350 (2008).
15. Q. L. Bao et al., "Atomic-layer graphene as a saturable absorber for ultrafast pulsed lasers," *Adv. Funct. Mater.* **19**(19), 3077–3083 (2009).
16. J. Jasaparal et al., "Simultaneous amplification and compression of picosecond pulses to 50 kW in Er fiber," in *European Conference on Lasers and Electro-Optics, 2007 and the International Quantum Electronics Conf. CLEOE-IQEC*, p. 1, IEEE (2007).
17. L. M. Zhao et al., "Dissipative soliton operation of an ytterbium-doped fiber laser mode locked with atomic multilayer graphene," *Opt. Lett.* **35**(21), 3622–3624 (2010).
18. Q. Wang et al., "All-fiber passively mode-locked thulium-doped fiber ring laser using optically deposited graphene saturable absorbers," *Appl. Phys. Lett.* **102**(13), 131114–131117 (2013).
19. A. Schmidt et al., "Passive mode locking of Yb:KLuW using a single-walled carbon nanotube saturable absorber," *Opt. Lett.* **33**(7), 729–731 (2008).
20. Y. W. Song et al., "1300-nm pulsed fiber lasers mode-locked by purified carbon nanotubes," *IEEE Photon. Tech. Lett.* **17**(8), 1623–1625 (2005).
21. X. Li et al., "Yb-doped passively mode-locked fiber laser based on a single wall carbon nanotubes wallpaper absorber," *Opt. Laser Technol.* **47**(0), 144–147 (2013).
22. Z. Yu, Y. Wang, and Y. Song, "The application of carbon nanotubes in mode locked fiber laser," *Proc. SPIE* **8923**, 89231F (2013).
23. J. Xu et al., "Dissipative soliton generation from a graphene oxide mode-locked Er-doped fiber laser," *Opt. Express* **20**(21), 23653–23658 (2012).
24. Z. Liu, X. He, and D. N. Wang, "Passively mode-locked fiber laser based on a hollow-core photonic crystal fiber filled with few-layered graphene oxide solution," *Opt. Lett.* **36**(16), 3024–3026 (2011).
25. F. Shohda et al., "A passively mode-locked femtosecond soliton fiber laser at 1.5 microm with a CNT-doped polycarbonate saturable absorber," *Opt. Express* **16**(26), 21191–21198 (2008).
26. C. Zhao et al., "Ultra-short pulse generation by a topological insulator based saturable absorber," *Appl. Phys. Lett.* **101**, 211106 (2012).
27. C. Zhao et al., "Wavelength-tunable picosecond soliton fiber laser with topological insulator: $\mathrm{Bi_2Se_3}$ as a mode locker," *Opt. Express* **20**(25), 27888–27895 (2012).
28. H. Zhang et al., "Molybdenum disulfide ($\mathrm{MoS_2}$) as a broadband saturable absorber for ultra-fast photonics," *Opt. Express* **22**(6), 7249–7260 (2014).
29. C. Rogers and W. F. Shadwick, *Backlund Transformations* Cambridge University Press, New York (1982).
30. E. M. E. Zayed, H. A. Zedan, and K. A. Gepreel, "Group analysis and modified tanh-function to find the invariant solutions and soliton solution for nonlinear Euler equations," *J. Nonlinear Sci. Numer. Simul.* **5**(3), 221–234 (2004).
31. M. Inc and D. J. Evans, "On travelling wave solutions of some nonlinear evolution equations," *J. Comput. Math.* **81**(2), 191–202 (2004).
32. J. Hu, "A new method of exact travelling wave solution for coupled nonlinear differential equations," *Phys. Lett. A* **322**(3–4), 211–216 (2004).
33. W. X. Ma and J. H. Lee, "A transformed rational function method and exact solutions to the $(3+1)$ dimensional JimboMiwa equation," *Chaos Solitons Fractals* **42**(3), 1356–1363 (2009).
34. H. Kumar and F. Chand, "Soliton solutions of complex modified KdV equation with time-dependent coefficients," *Indian J. Phys.* **87**(9), 909–912 (2013).
35. J. R. Costa and C. R. Paiva, "Modified split-step Fourier method for the numerical simulation of soliton amplification in erbium-doped fibers with forward propagating noise," *IEEE J. Quantum Electron.* **37**(1), 145–151 (2001).
36. G. P. Agrawal, *Application of Nonlinear Fiber Optics*, Academic Press, Elsevier, USA (2001).
37. C. Vinegoni, M. Wegmuller, and N. Gisin, "Measurements of the nonlinear coefficient of standard SMF, DSF, and DCF fibers using a self-aligned interferometer and a Faraday mirror," *IEEE Photonics Technol. Lett.* **13**(12), 1337–1339 (2001).
38. Á. Szabó and Z. Várallyay, "Numerical study on the saturable absorber parameter selection in an erbium fiber ring oscillator," *IEEE Photonics Technol. Lett.* **24**(2), 122–124 (2012).

39. X. Zhao et al., "Switchable, dual-wavelength passively mode-locked ultrafast fiber laser based on a single-wall carbon nanotube mode locker and intracavity loss tuning," *Opt. Express* **19**(2), 1168–1173 (2011).
40. A. Martinez et al., "Passive mode-locked lasing by injecting a carbon nanotube-solution in the core of an optical fiber," *Opt. Express* **18**(11), 11008–11014 (2010).
41. F. Ahmad et al., "A passively mode-locked erbium-doped fiber laser based on a single-wall carbon nanotube polymer," *Chin. Phys. Lett.* **30**(5), 054210 (2013).
42. I. A. Yarutkina et al., "Numerical modeling of fiber lasers with long and ultra-long ring cavity," *Opt. Express* **21**(10), 12942–12950 (2013).
43. M. Currie et al., "Mode-locked 2-μm wavelength fiber laser using a graphene-saturable absorber," *Opt. Eng.* **52**(7), 076101 (2013).

Younis Mohamed Atiah Al-zahy has been an associate professor of physics in the Department of Science at Misan University since 2006. He received a PhD and MSc degrees in the College of Physical Science from Al-Mustansiriya University, Iraq, in 2006 and 1998, respectively. Currently, he works at the Laboratory of Laser Technology, and the College of Science as a lecturer in physics. He has published many papers in the field of fiber lasers.